Remote estimation of pulse wave features related to arterial stiffness and blood pressure using a camera

Djamaleddine Djeldjli, Frédéric Bousefsaf, Choubeila Maaoui, Fethi Bereksi-Reguig, Alain Pruski

Remote Estimation of Pulse Wave Features Related to Arterial Stiffness and Blood Pressure Using a Camera

Djamaleddine Djeldjli[a,b], Frédéric Bousefsaf[a], Choubeila Maaoui[a], Fethi Bereksi-Reguig[b], Alain Pruski[a]

[a] *Université de Lorraine, LCOMS, F-57000 Metz, France*
[b] *Laboratoire de Génie Biomédical, Université de Tlemcen, 13000 Tlemcen, Algeria*

Abstract

Recent technological advances in the field of sensors, signal processing and image processing favor the development of new techniques for vital parameters monitoring such as imaging photoplethysmography (iPPG). iPPG is a simple and noninvasive measurement technique. It has been employed to remotely estimate heart and respiratory rates, oxygen saturation and blood pressure through the measurement of blood volume pulse using a camera. In the recent decades, researchers used the morphology of contact photoplethysmographic (cPPG) signal for the assessment of arterial stiffness, blood pressure, arteriosclerosis, cardiac output, and vascular aging. We propose to study, in this article, the similarities between iPPG and cPPG waveform features that are associated to cardiovascular diseases. A fast camera and contact probes were respectively employed to record iPPG and cPPG signals. Their waveform features such as time, areas, amplitude and second derivative features were then extracted and analyzed. Results show a high correlation between the two measurement techniques. This research opens several perspectives in the remote assessment of blood pressure and arterial stiffness, and therefore for non-contact diagnosis of several cardiovascular diseases.

Keywords: Imaging Photoplethysmography, Blood Volume Pulse, Waveform, Camera, Arterial Stiffness, Blood Pressure

1. Introduction

The continuous monitoring of vital parameters is an emerging concept in healthcare where the competition to seek a non-invasive, more effective, comfortable and less expensive technique has led to the wide use of photoplethysmography [1]. Using only a simple LED and a photoreceptor, it allows the measurement of the blood volume pulse (BVP) [2]. The contact photoplethysmographic (cPPG) signal is rich in information. Its periodicity reflects the heart rate while its waveform shape provides more information on cardiac hemodynamics, age and condition of blood vessels [1, 3, 4]. Despite its advantages, cPPG remains slightly uncomfortable due to the use of contact probes. Furthermore, its use is almost impossible in the case of trauma, skin ulcer, burns, congenital and contagious diseases [5, 6, 7, 8]. For example, very young children (before 27 weeks after birth) may suffer from skin lesions when using these sensors [9]. Also, the excessive pressure of the sensors on the skin can create a temporary occlusion of the subcutaneous capillaries and thus interfering with the measurement [10]. These limits have led the researchers to develop a new contactless technique [11, 5, 6, 7, 9, 5, 8].

Recently, imaging photoplethysmography (iPPG) has attracted a particular attention: its various qualities tend to overcome the drawbacks mentioned above while reducing the wiring and

increasing the patient's safety. iPPG is a technique based on the same principle as cPPG while it uses a camera and a dedicated light source, ambient light or daylight. It allows remote detection of BVP from human face images by tracking subtle changes in skin color that are not perceptible to the human eye. iPPG can be recorded using cameras embedded in daily use devices like smartphones or laptops. These technologies are low-cost and ubiquitous. Researchers focused on iPPG especially for the assessment of cardiac activity and respiratory monitoring [12, 13, 14, 15, 16]. It was also used for blood pressure measurement [17, 18, 19], oxygen saturation [20, 21, 22], skin detection [23] and mental stress assessment [24].

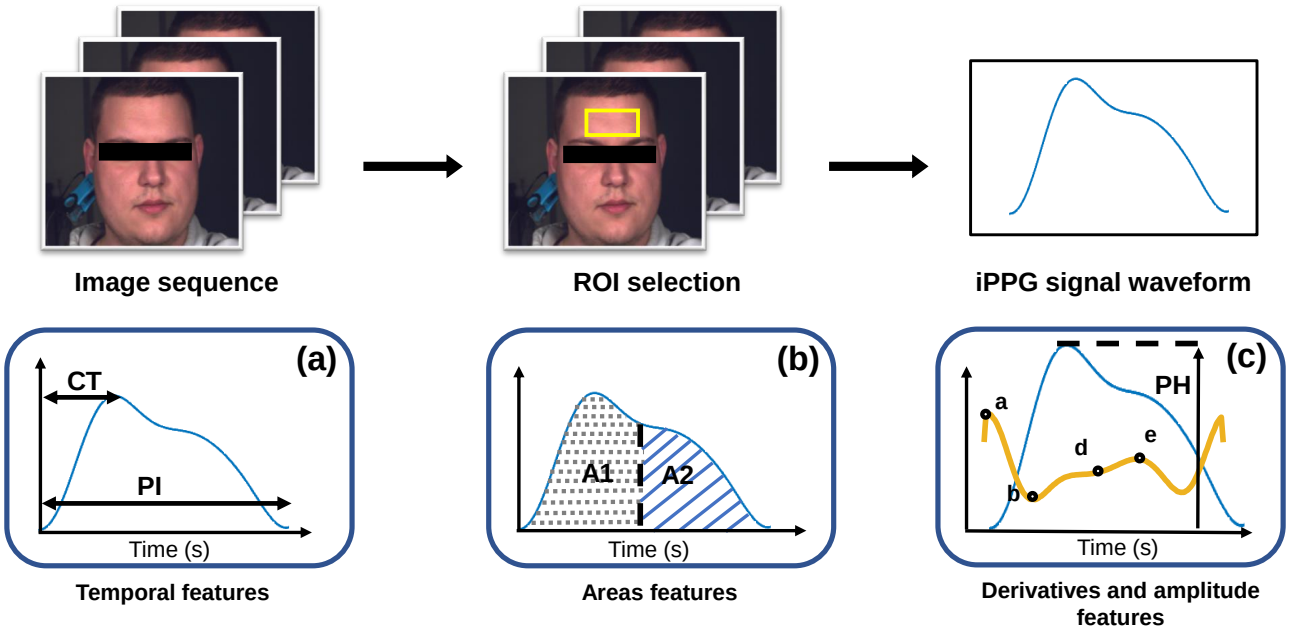

Figure 1: Proposed approach: image processing operations are applied on the video stream to detect the forehead as Region Of Interest (ROI). The signal is computed using a spatial averaging operation over the ROI before being processed by temporal filters. Finally, (a) temporal, (b) areas and (c) derivatives and amplitude features are estimated from this signal. These features are related to blood pressure, heart rate and arterial stiffness.

In this paper, we analyze iPPG waveforms extracted from a facial video in order to extract features associated with cardiac activity and hemodynamics (Figure 1). To the best of our knowledge, no articles have studied the similarity between features extracted from iPPG and cPPG signals. The proposed method is the first attempt to compute a set of parameters extracted from iPPG waveform measured by camera. The results of this research allow a knowledge deepening in the field of iPPG and particularly towards non-contact estimation of blood pressure, arterial stiffness and cardiac activity.

The rest of the paper is organized as follows: an overview of cPPG signal waveform features and their medical significance is presented in section 2. We describe, in a third section, the proposed method by giving details about the recording of iPPG signals and about the extraction of their relevant waveform features. Finally, the obtained results are discussed before presenting the conclusion and perspectives of this study.

2. Background

In this section a review of previous works on cPPG signal waveform features and their applications is presented since as far as our research literature in the domain showed no systematic study

on iPPG signal waveform analysis .

Several factors can affect the PPG signal waveform: the heart rate mainly depends on total pulse width while the physiological modifications of hemodynamic and arterioles properties are manifested as distortion in the waveform profiles [25]. Its analysis is also interesting especially for blood circulation assessment [26] and respiratory monitoring [27]. Usually waveform profile variations are very weak and difficult to handle. For this reason, researchers employed the derivatives of cPPG signal waveform to facilitate its analysis [28].

All the PPG features computed from the pulse waveform are shown in Figure 2. They are presented in three separate categories: temporal, areas, amplitude and derivative features.

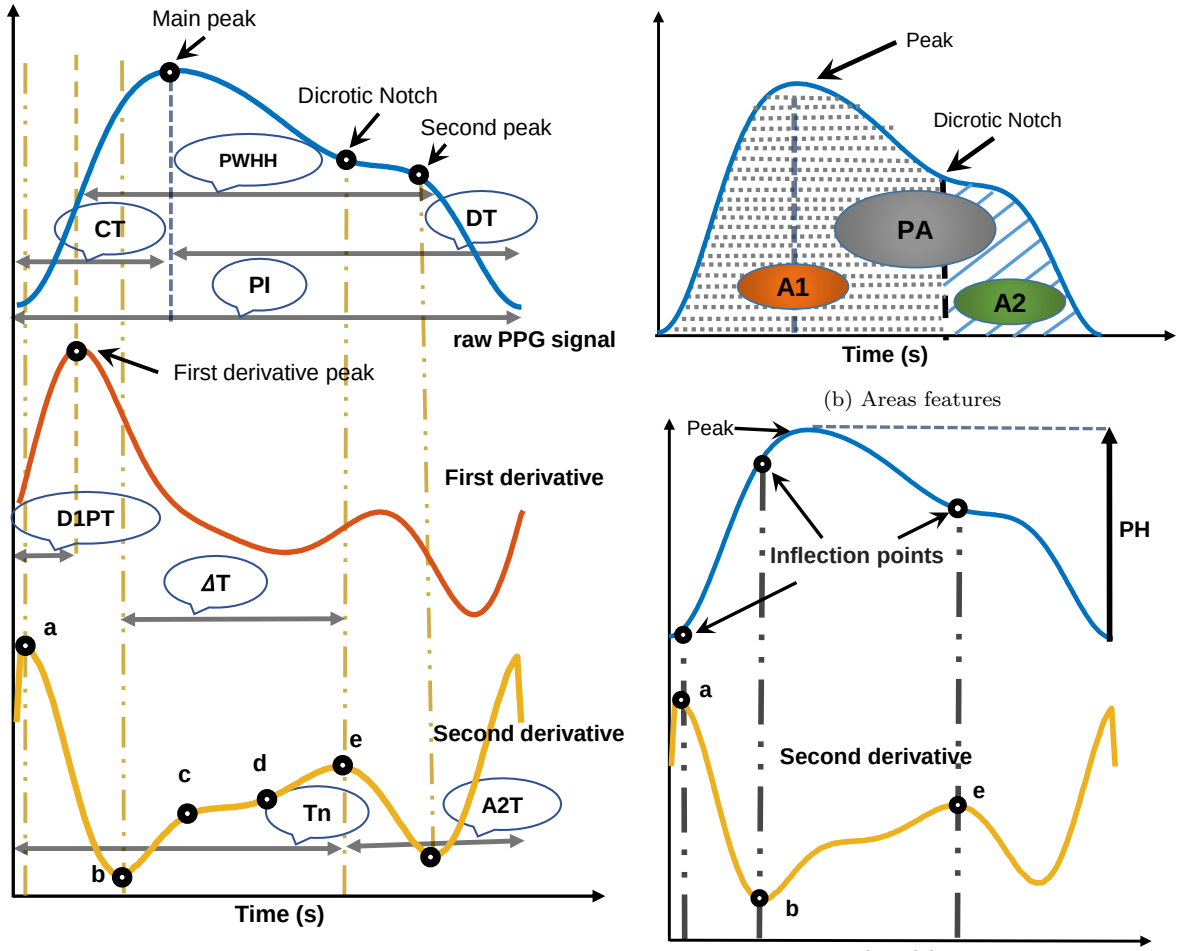

(a) Temporal features

(b) Areas features

(c) second derivatives and amplitude features

Figure 2: PPG waveform features presented in three categories: (a) temporal features, (b) area features and (c) second derivative and amplitude features. The derivatives are used to facilitate some features calculation.

2.1. Temporal features

Temporal features are represented in Figure 2a. Crest time (CT) is the time from the PPG wave foot to the systolic peak (main peak) [29, 30, 31]. Alty et al. [29] proved that CT can be a useful feature for cardiovascular diseases classification. CT increases with arteriosclerosis in particular for aged persons [31].

Pulse Interval (PI) is the time from the beginning to the end (foot to foot interval, see Figure 2a). It can replace peak to peak interval for pulse rate measurement [32]. The ratio between PI and pulse amplitude provides a good understanding of cardiovascular system properties [33]. Pulse interval is similar to R-R interval of ECG used for heart rate variability assessment [34].

ΔT is the time delay between the main systolic peak and the diastolic (secondary) peak. The inflection points are employed in the absence of a second peak or when the main peak is unclear [25, 35]. Millasseau et al. show that ΔT decreases with age as a consequence of increased large artery stiffness [36].

Pulse Width at the Half Height (PWHH) is the pulse width of PPG pulse at the half amplitude of the systolic peak (main peak) as shown in Figure 2a. Awad et al. suggested that PWHH is correlated with the systemic vascular resistance better than the systolic amplitude [37]. It is also correlated with blood pressure [38, 39].

Dicrotic Notch Time (Tn) is the time span between the starting point and dicrotic notch [30, 35, 40]. Wang et al. showed that Tn decreases with heavier exercise loads [30].

A2 Times (A2T) is the time span between notch point and the ending point of PPG waveform [35, 40]. Li et al. employed the time ratio of Tn to A2T to estimate blood pressure [40].

Diastolic Time (DT) corresponds to the time span from the PPG waveform main peak to its end [38]. Teng and Zhang found that DT is strongly correlated to blood pressure better than other features (CT, PI and PWHH) [38] .

First derivative peak time (FDPT) is the time span between the starting point and the peak of its first derivative [35]. It was used by Tanveer and Hasan with 12 PPG waveform features to propose a waveform-based hierarchical Long Short Term Memory model for BP estimation [35].

2.2. Areas

Features based on the pulse wave areas are presented in Figure 2b. Pulse Area (PA) corresponds to the total area under the PPG waveform curve [25, 30, 35]. The peripheral resistance, blood vessel elasticity and physiological changes in ejection function modify the total pulse area [30]. It also decreases with physical exercise [41]. Area 1 (A1) is the measured area from the beginning point to the dicrotic notch [30, 35]. It reflects the systolic characteristics of the pulse wave which are mainly influenced by cardiac ejection function [42]. Area 2 (A2) is the measured area from the dicrotic notch to the ending point [30, 35]. It reflects the diastolic characteristics of pulse wave which are affected by arterial compliance and peripheral resistance [43].

2.3. Amplitude and Derivatives

Features based on the pulse wave amplitude and its second derivative are presented in Figure 2c. Pulse Height (PH) is the amplitude of the main peak [30, 40, 44]. Von et al. [44] pointed out that the pulse amplitude is related to the left ventricular ejection performance, cardiac stroke volume and large artery distensibility, though the PPG pulse amplitude is associated with blood flow in small finger arteries. A high PH can indicate a high blood pressure, hyperthyroidism, fever, anemia, excessive blood volume, atherosclerosis, anxiety, and exercise. A low PH can indicate peripheral vasoconstriction, low blood pressure, hypovolemia, dehydration, hypothyroidism or increased peripheral resistance [44].

b/a is the ratio of b peak to a peak of the second derivative. Takazawa et al. demonstrated that the b/a ratio reflects increased arterial stiffness, hence the b/a ratio increases with age [28] . Imanaga et al. provided a direct evidence that magnitude of b/a is related to the peripheral artery distensibility, and suggest that the magnitude of b/a is a useful non-invasive index of atherosclerosis and altered arterial distensibility [45]. The ratio has also been employed to estimate the risk of a

cardiovascular disease [46]. e/a is the ratio of e peak to a peak of the second derivative. Takazawa et al. demonstrated that an increase of the e/a ratio reflects decreased arterial stiffness, and that the e/a ratio decreases with age [28]. Baek et al. confirmed that the e/a ratios decreases with age [47].

3. Materials and Methods

3.1. Experimental setup

12 voluntaries of both gender with different skin color, aged between 20 and 35 years old participated in this study. All procedures performed in this study were in accordance with ethical standards on human experimentation and with the 1964 Helsinki Declaration and its later amendments. Informed consent was obtained from all individual participants included in the study. None of them had any known cardiovascular disease.

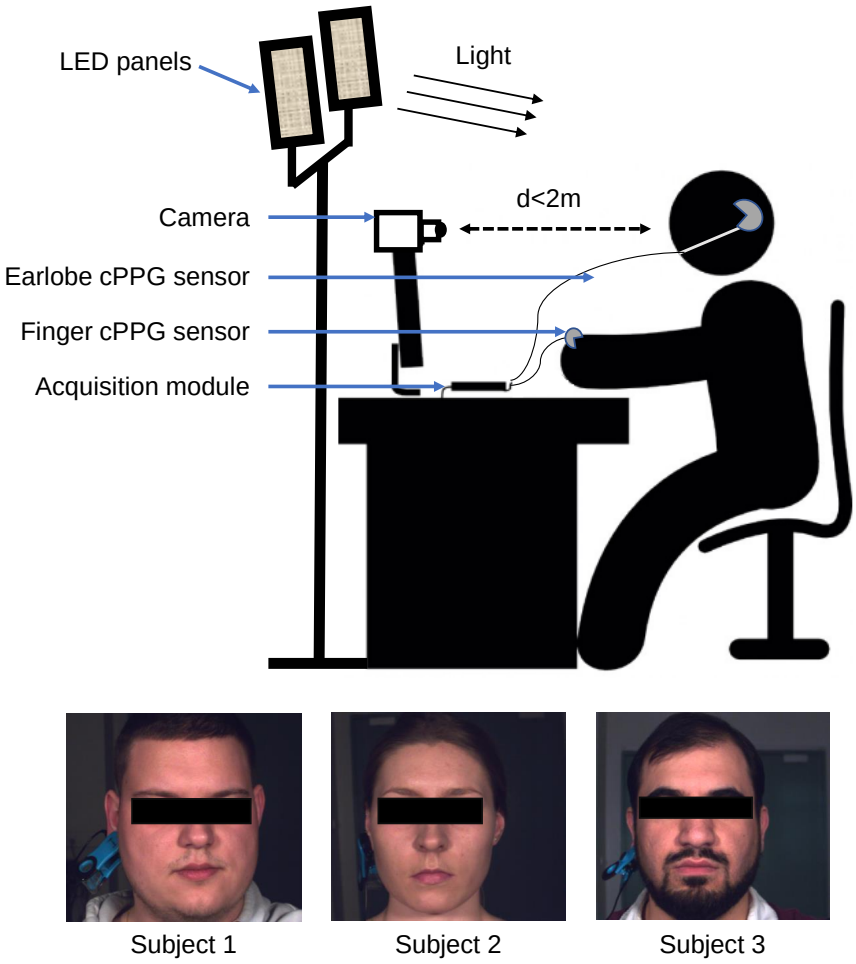

Figure 3: Experimental setup. The subject is seated in front of the camera at a distance of approximately 1m, two contact probes are placed on his/her ear and finger. The two LED panels are used as a controlled illumination source.

In the beginning of the experiments, the participants were asked to sit on a chair in front of the camera at approximately a distance of 1 m (Figure 3). Two contact PPG probes were placed ; one on the right earlobe and the other on the right index in order to record cPPG the ground

truth signals. The index finger has been chosen because most of literature studies have analyzed cPPG waveform from this particular area [25, 44]. Furthermore, earlobe has been chosen as a second reference because of its adjacency to the forehead (used as ROI for camera measurements). This way, we avoid placing the contact sensor on the forehead where it will partially occlude this area in the video stream. The two sensors were placed in two different sites to observe the effect of measurement site. During the recording, the participants were asked to keep Normal Breathing (NB) for 60 seconds and then asked to perform a Breath Hold (BH) as long as they can. Breath hold induces significant physiological variations.

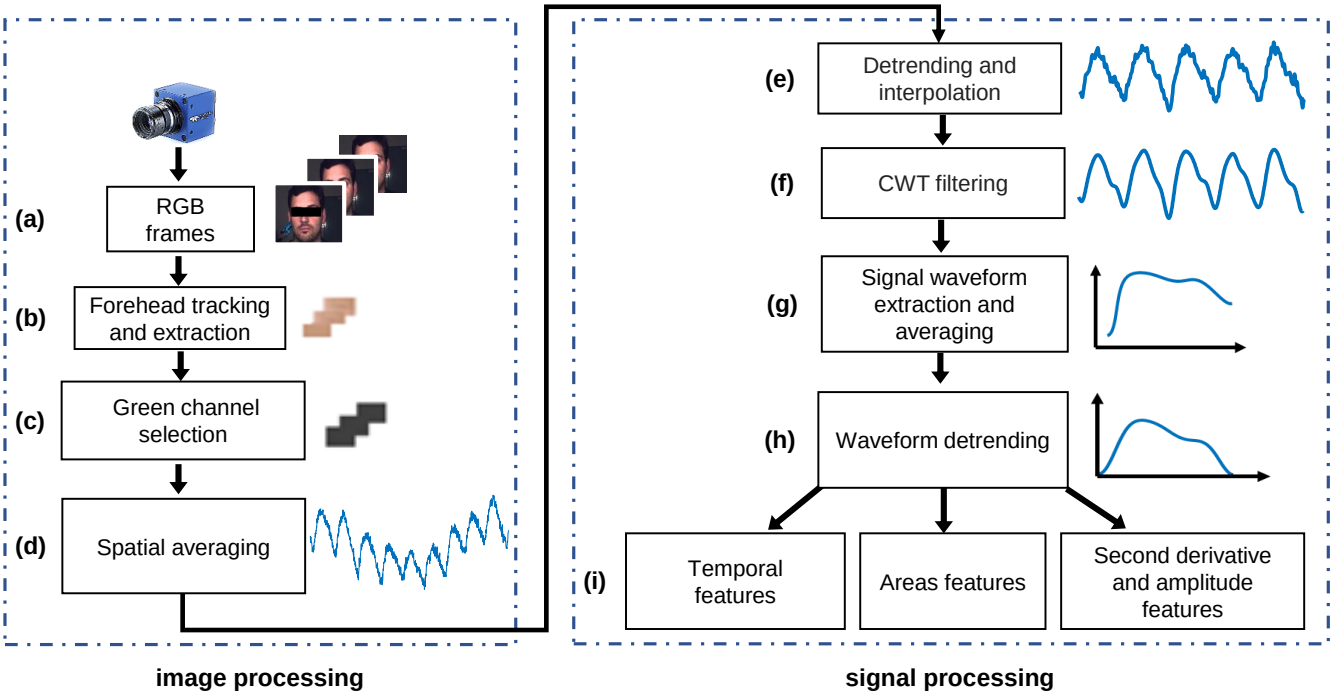

Figure 4: Overview of the proposed method. (a) Camera settings adjustment. (b) Forehead pixels are isolated for each frame by facial landmarks tracking. (c) Green Channel is selected from RGB color space. (d) Raw signal is extracted using a spatial averaging operation. Signal processing is performed by the following steps: (e) trends are removed and the signal is upsampled to a frequency of 256 Hz. (f) The signal is filtered and the valleys are detected. (g) The signal is processed wave by wave. Averaging of successive waves is proposed to ensure a better stability of the computed features. (h) Trends are removed to (i) precisely compute the features.

3.2. Materials

In this study, a fast camera (16mm C Series Lens mounted on a EO-2223C Color camera from Edmund Optics) has been used. The images were recorded using a C++ based software with a resolution of 640 $\times$ 480 pixels at a frame rate of 125 frames per second. The three channels composing the image (red, green and blue) are encoded with 8 bits per pixel. Images were saved in bmp format without any compression. The experiments were conducted in a dark room where the only source of light was two Neewer LED panels (NL480) as shown in Figure 3. LED illumination has been employed because it provides a stable and homogeneous lighting for iPPG measurement. The light intensity has been set to 80 % from a maximum of 3360 lux / m and the color temperature to 3750 K (neutral white light). Autoexposure and white balance have been disabled because they cause continuous regulation of image colors which generates artifacts in the extracted iPPG signals [14]. The raw extracted signals are processed offline using MATLAB (The MathWorks,

Inc.). For the results validation, two approved commercial PPG contact sensors (BVP-Flex / Pro. By Thought Technologies Ltd.) were employed. They use infrared light to record the ground-truth signal from the earlobe and the index at a sampling frequency of 256 Hz.

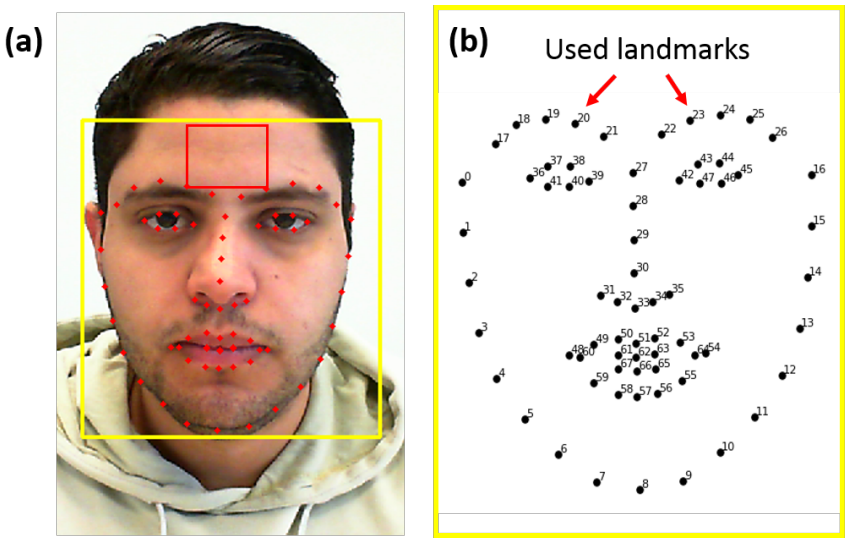

Figure 5: Forehead detection and tracking. (a) Forehead detection. The yellow and red rectangles respectively demarcate the detected face and forehead. The red dots correspond to the 68 facial landmarks. (b) The subset of landmarks used to track the forehead are indicated with red arrows.

3.3. iPPG signal extraction

The developed system, divided into two main parts, is presented in Figure 4. Camera parameters like zoom, brightness, contrast, exposure and color saturation were set in order to record a sequence of facial images suitable for iPPG signal extraction during the 60 seconds experiments. Dlib [1] and OpenCV [2] libraries were used for facial landmarks tracking (Figure 5) in order to isolate forehead pixels [48]. The forehead and cheeks areas are rarely covered by clothing or hair and correspond to ROIs with significant signal to noise ratio [49, 50]. Detecting facial landmarks in the images sequence was carried in two steps: first, the face detection was ensured by histogram of oriented gradients features combined with a linear classifier and a sliding window detection scheme [49]. Then a shape predictor is applied to localize 68 key points from the face region (eyes, eyebrows, nose, mouth, jawline) [48, 51]. For more stability, landmarks (68 coordinates per frame) of every 30 successive frames were averaged to get a single ensemble that can be applied on the current 30 successive facial images. Eyebrows landmarks are used to detect the forehead (Figure 5), which is used as the only region of interest [49].

No specific color transformation is used in this method: we employed the green channel (Figure 4c) of forehead area for iPPG signal extraction [11, 52].The raw iPPG signal is extracted from the pixels using a spatial averaging operation that transforms the pixels in the region of interest into a scalar [11]. This process is applied on a set of n frames to generate n scalars represented as a raw iPPG signal (Figure 4d).

The raw signal is firstly detrended using a smoothness priors approach (Figure 4e). We employed a time-varying finite impulse response high-pass filter [53, 52]. The signal is then resampled

[1] http://dlib.net/
[2] https://opencv.org/

at a frequency of 256 Hz by piecewise cubic hermite interpolating polynomial method [54] to accurately refine valleys. The resulting iPPG signal is then filtered using its continuous wavelet transform representation to retain the original waveform shape (Figure 4f) [14, 55]. We selected the bump wavelet and defined the bandwidth of the filter to [0.5–4.0] Hz. This step ensures proper determination of the iPPG signal waveform features. The contact PPG probes employed in this study (see section 3.2) deliver filtered PPG signals considered as ground truth.

3.4. Waveform features extraction

Both iPPG and cPPG filtered signals undergo the same processing. First and according to the signals valleys, we cut each wave alone in order to process the signals wave by wave [52]. Each wave was then independently re-interpolated to 256 points. In order to improve stability, every 10 successive pulse waves were averaged using a moving window (Figure 4g) and detrended (Figure 4h). Area, amplitude, second derivative and temporal features were then computed for each iPPG and cPPG pulse wave (Figure 4i) [52]. The extraction details of each feature has been described in section 2.

As shown in Figure 6a, natural discrepancies in the waveforms of each measurement site can be observed. These variations are produced by the differences in blood vessels density, by the interactions between probe and skin (e.g. local pressure) as well as by the inherent properties of skin [56]. Thus and in order to properly compare the results, each participant feature was normalized by considering the cPPG ear features as references. Equation 1 shows how the mean and standard deviation of each iPPG and cPPG finger features that are brought to a similar quantity as cPPG ear given feature:

3.5. Evaluation Metrics and Methods

The assessment of the proposed method is performed by a statistical analysis that relies on Pearson correlation coefficient as well as two types of errors: the Root Mean Square Error (RMSE, see equation 2) and the Mean Absolute Percentage Error (MAPE, see equation 3). The MAPE gives the accuracy of an estimation in regards to a reference value.

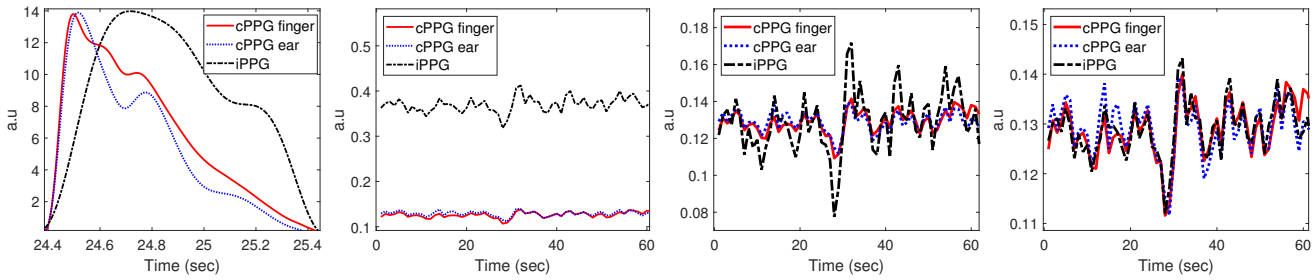

(a) Raw waveforms (b) Raw traces (c) Centered traces (d) Normalized traces

Figure 6: Raw pulse waves to normalized traces. (a) PPG excerpts extracted from the right earlobe and the right finger using contact probes and from the forehead using the camera frames. (b) Raw Crest Time (CT) feature traces extracted from the three measurement sites for several continuous PPG pulse waves. (c) CT traces brought to the same mean as CT of cPPG ear. (d) Normalized traces (same mean and standard deviation as cPPG ear). The evolution in the traces are very similar, showing that the two measurement techniques (contact probes and camera) can effectively assess this physiological parameter.

$$X_{norm} = \sigma_{cPPGear}\left(\frac{X - \mu_X}{\sigma_X}\right) + \mu_{cPPGear} \tag{1}$$

Where X_{norm} is a feature trace computed from iPPG or finger cPPG. μ and σ respectively correspond to the mean and standard deviation of a feature trace. X corresponds to either a iPPG or a finger cPPG feature trace.

$$RMSE = \sqrt{MSE} = \sqrt{\frac{\sum_{i=1}^{N} (Y_i - X_i)^2}{N}} \tag{2}$$

$$MAPE = \frac{100}{N} \sum_{i=1}^{N} \left| \frac{Y_i - X_i}{Y_i} \right| \tag{3}$$

N corresponds to the number of samples. X, the estimation, is either a finger cPPG or a iPPG normalized feature (equation 1). Y, the reference, is the corresponding cPPG normalized feature trace.

4. Results and Discussion

Previous studies [1, 25] show that cPPG waveform features are strongly related to several physiological parameters such as heart rate, respiratory rate, arterial stiffness, vessels aging and blood pressure (see section 2). We propose to compare contactless PPG signal waveform recorded using a camera with contact PPG probes.

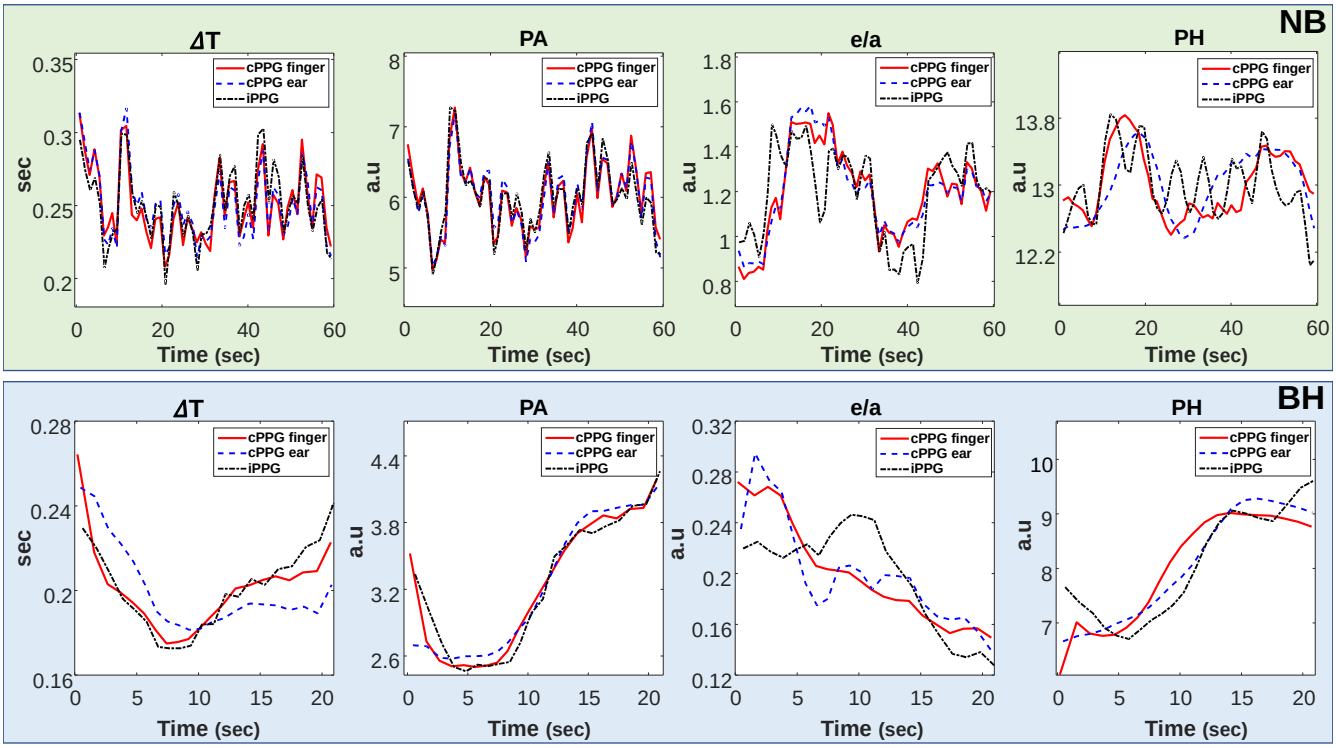

Figure 7: Each presented feature belongs to a specific category: ΔT (time delay between systolic and diastolic peaks) belongs to temporal features, PA (pulse area) belongs to area features, e/a corresponds to the ratio of the second derivative amplitudes of e and a points, PH (pulse height) is associated to the amplitudes. Each row represents the feature traces for a particular experiment: Normal Breathing (NB, top row) and Breath Hold (BH, bottom row). The traces were computed from the PPG signals of participant #1. Good agreement can be observed between the contact and non-contact series.

The features extracted from these waveforms were assessed and the obtained results are presented in Figure 7 and tables 1, 2 and 3. The features are divided into three categories: temporal, area, second derivative and amplitude (see figure 2). They are extracted from 3 different measurement sites, namely the forehead, using the camera, the right ear and the right index, using approved contact sensors. Furthermore, we compare the results from the two contact sensors measurements in order to observe the impact of the measurement sites [57] and to ensure that the errors are not due to the processing of the iPPG signals. To sum up, the analysis is done on 3 comparisons of features: iPPG forehead vs cPPG ear, iPPG forehead vs cPPG finger and cPPG ear vs cPPG finger.

Figure 7 presents an example of a feature per category. We note that the three traces evolve in the same way and that breath hold induces significant physiological variations.

4.1. Temporal features

The 8 temporal features are frequently employed in the literature for the assessment of several physiological parameters [25]. Table 1 shows the comparison between the camera and the contact probes. We also present, in Figure 8, scatterplots of 3 features were selected according to their degree of correlation where one can notice that compared signals show a high correlation in the DT feature (0.92 for NB and 0.90 for BH), a good correlation in the A2T feature (0.88 for NB and 0.81 for BH) and an acceptable correlation in the PWHH feature (0.81 for NB and 0.73 for BH).

Table 1: Statistical analysis of temporal features. PI is the pulse interval, PWHH is the pulse width at the half height, FDPT is the first derivative peak time, A2T is the second area time, TN is the dicrotic notch time, ΔT is the time delay between the systolic and diastolic peaks, CT is the crest time and DT is the diastolic time. p-values are $< 10^{-4}$ for all correlation coefficients. RMSE corresponds to the Root Mean Square Error and MAPE to the Mean Absolute Percentage Error.

		$cPPG_{ear}$ vs iPPG			**$cPPG_{finger}$ vs iPPG**			**$cPPG_{finger}$ vs $cPPG_{ear}$**		
Feat.	**Exp.**	**Correlation** $\mu \pm \sigma$	**RMSE** (sec)	**MAPE** (%)	**Correlation** $\mu \pm \sigma$	**RMSE** (sec)	**MAPE** (%)	**Correlation** $\mu \pm \sigma$	**RMSE** (sec)	**MAPE** (%)
PI	NB	**0.93** $\pm$ 0.05	0.02	1.46	**0.89** $\pm$ 0.09	0.02	1.58	**0.96** $\pm$ 0.09	0.01	0.53
	BH	**0.90** $\pm$ 0.07	0.03	2.35	**0.84** $\pm$ 0.14	0.04	2.68	**0.90** $\pm$ 0.13	0.03	1.33
PWHH	NB	**0.81** $\pm$ 0.12	0.01	2.46	0.56 $\pm$ 0.33	0.02	3.63	0.63 $\pm$ 0.36	0.02	3.12
	BH	**0.73** $\pm$ 0.17	0.03	5.16	0.52 $\pm$ 0.29	0.04	7.89	0.54 $\pm$ 0.46	0.03	6.81
FDPT	NB	**0.78** $\pm$ 0.11	0.00	2.97	**0.73** $\pm$ 0.13	0.00	3.14	**0.74** $\pm$ 0.17	0.00	3.29
	BH	**0.73** $\pm$ 0.09	0.00	4.49	**0.70** $\pm$ 0.33	0.00	4.06	**0.73** $\pm$ 0.27	0.00	3.68
T2A	NB	**0.88** $\pm$ 0.06	0.02	2.08	**0.82** $\pm$ 0.14	0.02	2.42	**0.91** $\pm$ 0.15	0.01	1.13
	BH	**0.84** $\pm$ 0.11	0.03	3.55	**0.78** $\pm$ 0.13	0.04	3.81	**0.90** $\pm$ 0.09	0.02	1.81
TN	NB	**0.85** $\pm$ 0.08	0.01	2.24	**0.75** $\pm$ 0.15	0.01	2.76	**0.84** $\pm$ 0.18	0.01	1.85
	BH	**0.81** $\pm$ 0.10	0.02	4.09	**0.66** $\pm$ 0.19	0.02	5.01	**0.80** $\pm$ 0.18	0.01	3.24
ΔT	NB	**0.80** $\pm$ 0.11	0.01	2.85	0.64$\pm$ 0.17	0.01	3.57	**0.80** $\pm$ 0.20	0.01	2.31
	BH	**0.78** $\pm$ 0.14	0.02	4.95	0.57 $\pm$ 0.19	0.02	6.24	**0.66** $\pm$ 0.23	0.01	5.03
CT	NB	**0.79**$\pm$ 0.11	0.00	2.66	**0.67** $\pm$ 0.26	0.01	3.04	**0.76** $\pm$ 0.27	0.00	2.29
	BH	**0.79** $\pm$ 0.13	0.02	5.67	0.62 $\pm$ 0.35	0.02	7.10	**0.78** $\pm$ 0.22	0.01	3.57
DT	NB	**0.92** $\pm$ 0.05	0.02	1.55	**0.88** $\pm$ 0.10	0.02	1.67	**0.95** $\pm$ 0.10	0.01	0.66
	BH	**0.90** $\pm$ 0.07	0.03	2.39	**0.84** $\pm$ 0.12	0.04	2.84	**0.90** $\pm$ 0.12	0.03	1.39

We notice that the temporal features are very well correlated (e.g. ΔT in Figure 7), in particular for the two comparisons cPPG ear vs cPPG finger and iPPG vs cPPG ear. Also, we notice that

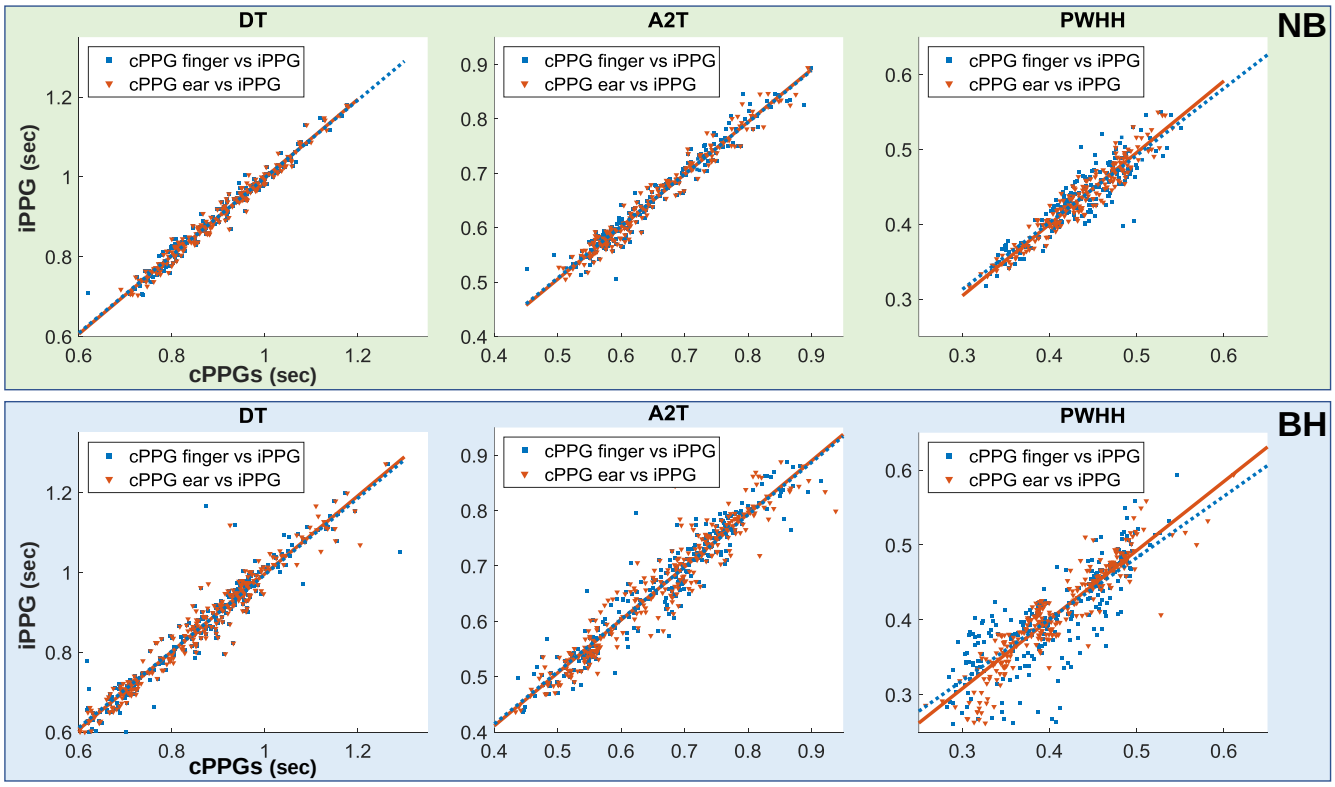

Figure 8: Scatterplot with representations of three temporal features: DT: Diastolic Time, A2T: time of second area, PWHH: Pulse Width at the Half Height. Non-contact measurements are in good agreement with contact ones for DT and A2T. Correlations presented in table 1 reflect this observation. The lines of identity show the line of best fit.

PI and DT present the best correlations. For the three comparisons the correlation varies between 0.84 and 0.96 for both experiments. PWHH exhibits a lower correlation than the rest of the features. It remains acceptable if we consider only the comparison iPPG vs cPPG ear where it reaches 0.73 for BH and 0.81 for NB. Note that in all temporal features the correlation for NB is higher than for BH while MAPE and RMSE values follow an inverse pattern: they are higher for BH than for NB.

The parameters extracted from cPPG ear are very well correlated with iPPG ones compared to those extracted from the finger. It clearly reflects the significant impact of the measurement site on the correlations since the forehead and the ear are very close in terms of ROI compared to the finger. The low errors values and slope of the fitting line in the scatterplots as well as a low p-values ($< 10^{-4}$)indicate a strong relationship between the two measurement techniques.

4.2. Area features

Area features are generally related to vessel properties such as resistance, elasticity and compliance. They are also exploited to characterize the ventricular ejection properties [30].

Table 2 shows that the two comparisons iPPG vs cPPG ear and cPPG ear vs cPPG finger exhibit comparable correlation values for all area features. PA evolves in the same way for all measurement sites. Note that BH introduces a significant change in these features (see Figure 7 for a typical example). In contrast with the temporal features, the correlation in the case of BH is better than for NB experiment. We suppose that these lower correlation values are associated with the magnitude of the physiological changes: no significant physiological changes related to the

Table 2: Statistical analysis of area features. PA: pulse area, A1: area before the dicrotic notch, A2: area after dicrotic notch. p-values are $< 10^{-4}$ for all correlation coefficients.

		$\mathbf{cPPG_{ear}}$ **vs iPPG**			$\mathbf{cPPG_{finger}}$ **vs iPPG**			$\mathbf{cPPG_{finger}}$ **vs** $\mathbf{cPPG_{ear}}$		
Feat.	**Exp.**	**Correlation** $\mu \pm \sigma$	**RMSE**	**MAPE** (%)	**Correlation** $\mu \pm \sigma$	**RMSE**	**MAPE** (%)	**Correlation** $\mu \pm \sigma$	**RMSE**	**MAPE** (%)
PA	NB	**0.75** $\pm$ 0.17	0.16	3.57	0.55 $\pm$ 0.34	0.21	4.64	0.61 $\pm$ 0.28	0.17	4.24
	BH	**0.87** $\pm$ 0.17	0.16	4.23	**0.88** $\pm$ 0.07	0.17	4.78	**0.87** $\pm$ 0.11	0.15	4.36
A1	NB	**0.68** $\pm$ 0.15	0.11	4.30	0.46$\pm$ 0.39	0.12	5.16	0.51 $\pm$ 0.32	0.11	4.90
	BH	**0.81** $\pm$ 0.22	0.10	5.24	**0.86** $\pm$ 0.09	0.11	5.62	**0.85** $\pm$ 0.13	0.10	5.34
A2	NB	**0.68** $\pm$ 0.15	0.10	4.74	0.50 $\pm$ 0.34	0.11	5.40	**0.67** $\pm$ 0.31	0.08	3.97
	BH	**0.80** $\pm$ 0.15	0.12	6.26	**0.78** $\pm$ 0.15	0.12	6.84	**0.85** $\pm$ 0.12	0.10	4.97

vessel properties appear at rest. A breath hold, however, produces a global change in physiology that induces significant variations in the pulse wave areas.

For all area features, the comparison cPPG ear vs iPPG shows a higher correlation than the other comparisons. We believe that this observation is a consequence of the measurement sites, the ear being closer to the forehead than the finger. The slope of the fitting line in the scatterplots (Figure 9) as well as the RMSE and MAPE values show a strong relationship between the measurement techniques. Note that the areas are particularly sensitive to camera noise and motions artifacts.

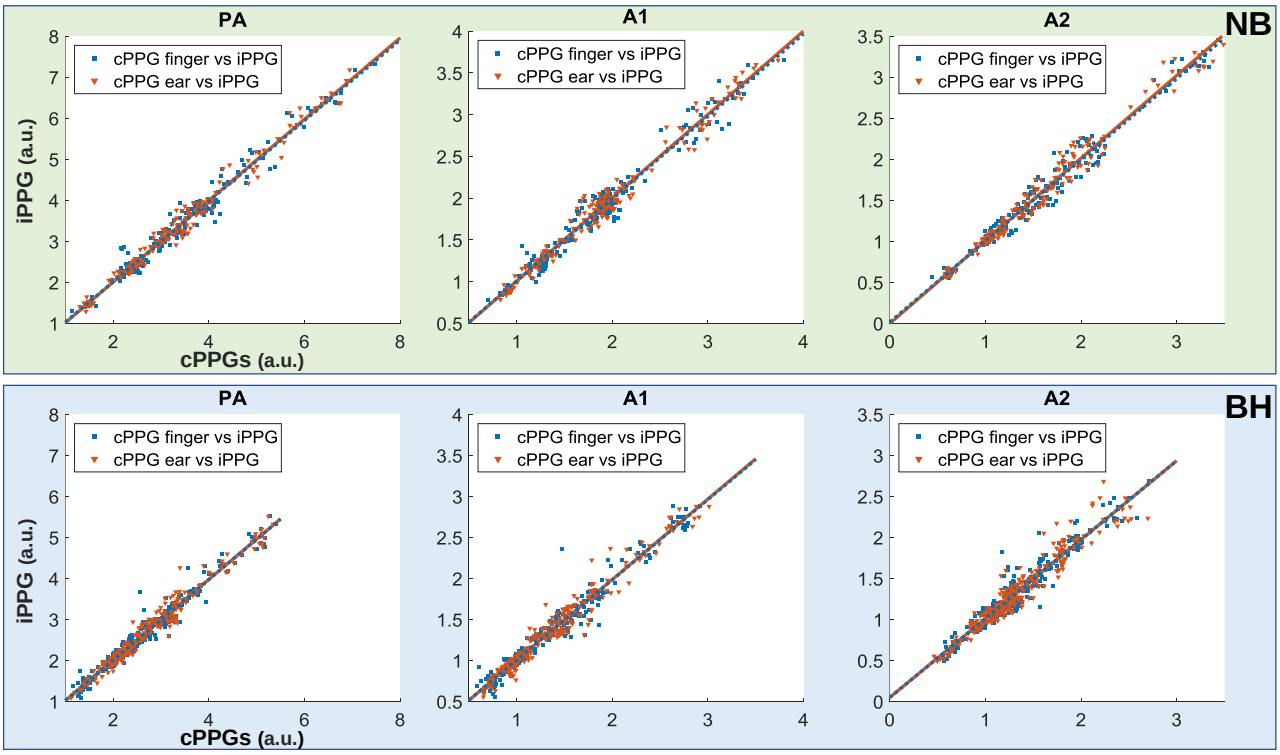

Figure 9: Scatterplot representations for area features. PA: Pulse Area, A1: area before the dicrotic notch, A2: area after dicrotic notch, for the two experiments NB (normal breathing) and BH (breath hold). The lines of identity show the line of best fit.

4.3. Second derivative and amplitude features

The second derivative reflects the finest variations of the pulse waveform. This parameter is mainly associated with arterial stiffness and therefore ageing [25].

From table 3 and the scatterplots (Figure 10), we notice that RMSE and MAPE are acceptable, but correlations are somewhat low. Only the comparison iPPG vs cPPG ear exhibits an average correlation. Note that this parameter is very sensitive to artifacts where slight perturbations in the iPPG waveform can drastically affect the features computed from its second derivative. In practice, this effect tends to produce strong outliers that lead to a drop in correlation. We also suppose that second derivative features are closely related to blood vessels density and to vascular properties (e.g. vessels aging) which differ from one measurement site to another [56, 57].

Table 3: Statistical analysis of second derivative and amplitude features. b/a and e/a are the ratios of the second derivative amplitudes, PH is the Pulse height. p-values are $< 10^{-4}$ for all correlation coefficients.

		$cPPG_{ear}$ vs iPPG			**$cPPG_{finger}$ vs iPPG**			**$cPPG_{finger}$ vs $cPPG_{ear}$**		
Feat.	**Exp.**	**Correlation** $\mu \pm \sigma$	**RMSE**	**MAPE** (%)	**Correlation** $\mu \pm \sigma$	**RMSE**	**MAPE** (%)	**Correlation** $\mu \pm \sigma$	**RMSE**	**MAPE** (%)
b/a	NB	0.55 ± 0.26	0.03	2.40	0.14 ± 0.44	0.04	3.51	0.05 ± 0.42	0.04	3.79
	BH	**0.72** ± 0.15	0.04	3.55	0.11 ± 0.50	0.08	6.60	0.14 ± 0.65	0.08	6.39
e/a	NB	**0.60** ± 0.18	0.01	6.46	0.33 ± 0.45	0.02	8.53	**0.65** ± 0.36	0.02	5.37
	BH	**0.67** ± 0.17	0.03	22.90	0.24 ± 0.56	0.04	22.95	0.48 ± 0.57	0.03	18.03
PH	NB	0.22 ± 0.50	0.39	3.82	0.24 ± 0.42	0.39	3.99	0.28 ± 0.54	0.31	3.35
	BH	**0.80** ± 0.20	0.36	3.87	**0.83** ± 0.08	0.36	4.23	**0.79** ± 0.29	0.33	3.82

The correlations are good for BH experiments (around 0.70) and acceptable (around 0.57) for NB. According to Figure 7, e/a feature evolves in the same way. The Figure also exhibits the impact of a breath hold which induces a significant change of this feature.

PH is a rather special feature that depends on local vasodilation and vasoconstriction, two physiological processes that are induced by thermoregulation or variations in blood pressure [44]. In table 3 and Figure 10, all comparisons exhibit a strong correlation for the BH experiment (around 0.80) and a very weak correlation for NB (around 0.25). Figure 7 clearly reflects this observation. It should be noted that PH is almost constant at rest. In contrast, BH experiments caused significant variations of PH, which result in better correlation values.

The results presented in this study show that employing a camera to remotely measure cardiovascular parameters based on the PPG pulse waveform is very promising. Nearly all the contactless features are well correlated with those obtained using contact PPG probes even though both technologies are different. The discrepancies may be due to the difference in properties of the measurement sites [57]. We emphasize that several sources of noise can affect the iPPG signal such as camera (quantum efficiency), lighting or subject motions. We assume in this study that the effects of subtle and involuntary motions induced by heartbeat (ballistocardiographic effect) on the iPPG signal are very weak or even negligible as proved in [58].

In the light of the recent researches [59, 60], we must note that the physiological origin of the PPG modulation is still under debate and there is no consensus for a unique definition. According to the present results and independently of the origin of the phenomenon, it seems that iPPG (associated to white illumination) can be employed to remotely assess several cardiovascular properties. Our group recently proposed a method for assessing the peripheral vasomotor activity which is reflected by the modification of the pulsatile amplitudes in iPPG signals [12]. These changes are directly related to vessels state, either to vasoconstriction or vasodilation.

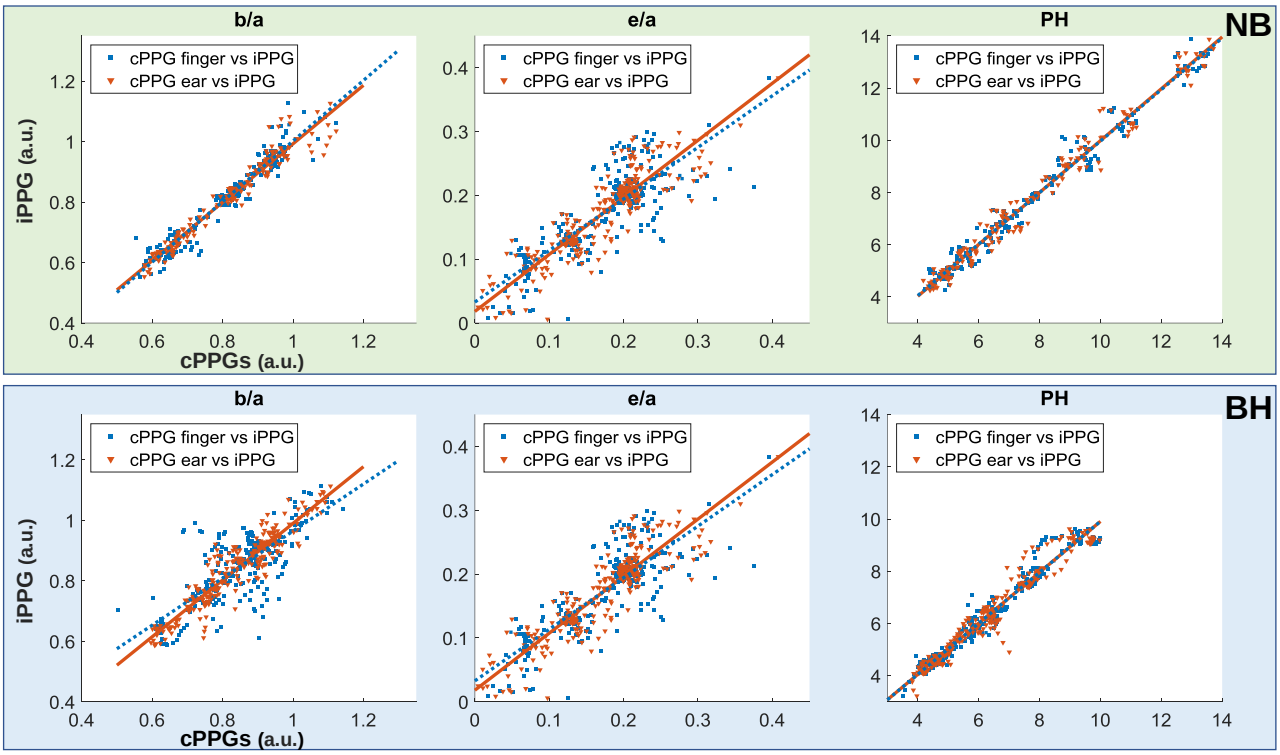

Figure 10: Scatterplot representations for second derivative and amplitude features.The lines of identity show the line of best fit.

5. Conclusion

Imaging photoplethysmography is a noninvasive, low cost, simple and contactless optical measurement technique employed to measure physiological parameters. We demonstrated, in this study, the feasibility of assessing iPPG waveform features remotely. The variations of these parameters are in close relation with several cardiovascular diseases such as arterial stiffness, blood pressure, and vascular aging. It provides a quantitative information to well understand the underlying mechanisms of waveform shape from different body sites. Contactless PPG features were compared to contact PPG features from two different sites. Several similarities and a strong correlation for two experiments (normal breathing and breath-holding) has been demonstrated. Therefore contact ear PPG and iPPG show a high correlation in temporal features, a good correlation in areas and an acceptable correlation for amplitude and derivative features. The measurement site effects can be the reason of the slight low correlation of some features. The results show that technologies employed to remotely measure PPG signals are of particular interest for the assessment of arterial stiffness, blood pressure and consequently for non-contact diagnosis of several cardiovascular diseases. The main limitations of this study are related to the small and constrained sample size (age and skin types). Thus, we plan to conduct similar experiments on a large-scale population including patients and elderly participants. In order to fully understand the effect of the measurement site we propose, as future work, to study the similarities between forehead cPPG and forehead iPPG waveforms by positioning a sensor specifically designed for cPPG forehead measurement. The effect of the wavelength range will be also analyzed through a comparison between contact and non-contact signals measured at the same and at different wavelengths (namely IR and green). This experience could subsequently be replicated in other areas of the body (e.g. hand region).

References

[1] J. Allen, Photoplethysmography and its application in clinical physiological measurement, Physiological measurement 28 (2007) R1–R39.

[2] A. Challoner, Photoelectric plethysmography for estimating cutaneous blood flow, Non-invasive physiological measurements 1 (1979) 125–151.

[3] L. A. Bortolotto, J. Blacher, T. Kondo, K. Takazawa, M. E. Safar, Assessment of vascular aging and atherosclerosis in hypertensive subjects: second derivative of photoplethysmogram versus pulse wave velocity, American Journal of Hypertension 13 (2000) 165–171. URL: https://academic.oup.com/ajh/article-lookup/doi/10.1016/S0895-7061(99)00192-2. doi:10.1016/S0895-7061(99)00192-2.

[4] N. Miyai, K. Miyashita, M. Arita, I. Morioka, K. Kamiya, S. Takeda, Noninvasive assessment of arterial distensibility in adolescents using the second derivative of photoplethysmogram waveform, European Journal of Applied Physiology 86 (2001) 119–124. URL: http://link.springer.com/10.1007/s004210100520. doi:10.1007/s004210100520.

[5] E. Gambi, M. Ricciuti, S. Spinsante, Sensitivity of the contactless videoplethysmography-based heart rate detection to different measurement conditions, in: 2018 26th European Signal Processing Conference (EUSIPCO), IEEE, 2018, pp. 767–771.

[6] L. Iozzia, L. Cerina, L. T. Mainardi, Assessment of beat-to-beat heart rate detection method using a camera as contactless sensor, in: 2016 38th Annual International Conference of the IEEE Engineering in Medicine and Biology Society (EMBC), IEEE, 2016, pp. 521–524.

[7] F. Bousefsaf, Mesure sans contact de l'activité cardiaque par analyse du flux vidéo issu d'une caméra numérique: extraction de paramètres physiologiques et application à l'estimation du stress, Ph.D. thesis, 2014.

[8] S. Bobbia, Vers le développement d'un capteur photopléthysmographique sans contact, Ph.D. thesis, 2019.

[9] J. M. Kuller, Skin breakdown: risk factors, prevention, and treatment, Newborn and Infant Nursing Reviews 1 (2001) 35–42.

[10] A. C. M. Dassel, R. Graaff, A. Meijer, W. G. Zijlstra, J. G. Aarnoudse, Reflectance pulse oximetry at the forehead of newborns: The influence of varying pressure on the probe, Journal of clinical monitoring 12 (1996) 421–428.

[11] W. Verkruysse, L. O. Svaasand, J. S. Nelson, Remote plethysmographic imaging using ambient light., Optics express 16 (2008) 21434–21445.

[12] F. Bousefsaf, C. Maaoui, A. Pruski, Peripheral vasomotor activity assessment using a continuous wavelet analysis on webcam photoplethysmographic signals, Bio-Medical Materials and Engineering 27 (2016) 527–538. doi:10.3233/BME-161606.

[13] W. Wang, A. C. den Brinker, S. Stuijk, G. de Haan, Algorithmic principles of remote ppg, IEEE Transactions on Biomedical Engineering 64 (2016) 1479–1491.

[14] F. Bousefsaf, C. Maaoui, A. Pruski, Continuous wavelet filtering on webcam photoplethysmographic signals to remotely assess the instantaneous heart rate, Biomedical Signal Processing and Control 8 (2013) 568–574.

[15] M.-Z. Poh, D. J. McDuff, R. W. Picard, Advancements in Noncontact, Multiparameter Physiological Measurements Using a Webcam, IEEE Transactions on Biomedical Engineering 58 (2011) 7–11. URL: http://ieeexplore.ieee.org/document/5599853/. doi:10.1109/TBME.2010.2086456.

[16] R. Macwan, Y. Benezeth, A. Mansouri, Heart rate estimation using remote photoplethysmography with multi-objective optimization, Biomedical Signal Processing and Control 49 (2019) 24–33.

[17] I. C. Jeong, J. Finkelstein, Introducing contactless blood pressure assessment using a high speed video camera, Journal of medical systems 40 (2016) 77.

[18] N. Sugita, M. Yoshizawa, M. Abe, A. Tanaka, N. Homma, T. Yambe, Contactless Technique for Measuring Blood-Pressure Variability from One Region in Video Plethysmography, Journal of Medical and Biological Engineering (2018) 1–10.

[19] X. Fan, Q. Ye, X. Yang, S. D. Choudhury, Robust blood pressure estimation using an RGB camera, Journal of Ambient Intelligence and Humanized Computing (2018). URL: http://link.springer.com/10.1007/s12652-018-1026-6. doi:10.1007/s12652-018-1026-6.

[20] D. Shao, C. Liu, F. Tsow, Y. Yang, Z. Du, R. Iriya, H. Yu, N. Tao, Noncontact monitoring of blood oxygen saturation using camera and dual-wavelength imaging system, IEEE Transactions on Biomedical Engineering 63 (2016) 1091–1098.

[21] A. R. Guazzi, M. Villarroel, J. Jorge, J. Daly, M. C. Frise, P. A. Robbins, L. Tarassenko, Non-contact measurement of oxygen saturation with an RGB camera, Biomedical Optics Express 6 (2015) 3320. URL: https://www.osapublishing.org/abstract.cfm?URI=boe-6-9-3320. doi:10.1364/BOE.6.003320.

[22] U. Bal, Non-contact estimation of heart rate and oxygen saturation using ambient light, Biomedical Optics Express 6 (2015) 86. URL: https://www.osapublishing.org/abstract.cfm?URI=boe-6-1-86. doi:10.1364/BOE.6.000086.

[23] S. Bobbia, R. Macwan, Y. Benezeth, A. Mansouri, J. Dubois, Unsupervised skin tissue segmentation for remote photoplethysmography, Pattern Recognition Letters 124 (2019) 82–90.

[24] F. Bousefsaf, C. Maaoui, A. Pruski, Remote assessment of physiological parameters by non-contact technologies to quantify and detect mental stress states, in: 2014 International Conference on Control, Decision and Information Technologies (CoDIT), IEEE, 2014, pp. 719–723.

[25] M. Elgendi, On the analysis of fingertip photoplethysmogram signals, Current cardiology reviews 8 (2012) 14–25.

[26] A. Reisner, P. A. Shaltis, D. McCombie, H. H. Asada, Utility of the photoplethysmogram in circulatory monitoring, Anesthesiology: The Journal of the American Society of Anesthesiologists 108 (2008) 950–958.

[27] L. Nilsson, A. Johansson, S. Kalman, Respiration can be monitored by photoplethysmography with high sensitivity and specificity regardless of anaesthesia and ventilatory mode, Acta anaesthesiologica scandinavica 49 (2005) 1157–1162.

[28] K. Takazawa, N. Tanaka, M. Fujita, O. Matsuoka, T. Saiki, M. Aikawa, S. Tamura, C. Ibukiyama, Assessment of vasoactive agents and vascular aging by the second derivative of photoplethysmogram waveform, Hypertension 32 (1998) 365–370.

[29] S. R. Alty, N. Angarita-Jaimes, S. C. Millasseau, P. J. Chowienczyk, Predicting arterial stiffness from the digital volume pulse waveform, IEEE Transactions on Biomedical Engineering 54 (2007) 2268–2275.

[30] A. Wang, L. Yang, W. Wen, S. Zhang, D. Hao, S. G. Khalid, D. Zheng, Quantification of radial arterial pulse characteristics change during exercise and recovery, The Journal of Physiological Sciences 68 (2018) 113–120.

[31] H.-T. Wu, C.-C. Liu, P.-H. Lin, H.-M. Chung, M.-C. Liu, H.-K. Yip, A.-B. Liu, C.-K. Sun, Novel application of parameters in waveform contour analysis for assessing arterial stiffness in aged and atherosclerotic subjects, Atherosclerosis 213 (2010) 173–177. URL: https://linkinghub.elsevier.com/retrieve/pii/S0021915010007239. doi:10.1016/j.atherosclerosis.2010.08.075.

[32] E. Gil, M. Orini, R. Bailon, J. M. Vergara, L. Mainardi, P. Laguna, Photoplethysmography pulse rate variability as a surrogate measurement of heart rate variability during non-stationary conditions, Physiological measurement 31 (2010) 1271.

[33] C. Poon, X. Teng, Y. Wong, C. Zhang, Y. Zhang, Changes in the photoplethysmogram waveform after exercise, in: 2004 2nd IEEE/EMBS International Summer School on Medical Devices and Biosensors, IEEE, 2004, pp. 115–118.

[34] S. Lu, H. Zhao, K. Ju, K. Shin, M. Lee, K. Shelley, K. H. Chon, Can Photoplethysmography Variability Serve as an Alternative Approach to Obtain Heart Rate Variability Information?, Journal of Clinical Monitoring and Computing 22 (2008) 23–29. URL: http://link.springer.com/10.1007/s10877-007-9103-y. doi:10.1007/s10877-007-9103-y.

[35] M. S. Tanveer, M. K. Hasan, Cuffless blood pressure estimation from electrocardiogram and photoplethysmogram using waveform based ANN-LSTM network, Biomedical Signal Processing and Control 51 (2019) 382–392.

[36] S. C. Millasseau, R. Kelly, J. Ritter, P. Chowienczyk, Determination of age-related increases in large artery stiffness by digital pulse contour analysis, Clinical science 103 (2002) 371–377.

[37] A. A. Awad, A. S. Haddadin, H. Tantawy, T. M. Badr, R. G. Stout, D. G. Silverman, K. H. Shelley, The relationship between the photoplethysmographic waveform and systemic vascular resistance, Journal of Clinical Monitoring and Computing 21 (2007) 365–372. URL: http://link.springer.com/10.1007/s10877-007-9097-5. doi:10.1007/s10877-007-9097-5.

[38] X. Teng, Y. Zhang, Continuous and noninvasive estimation of arterial blood pressure using a photoplethysmographic approach, in: Proceedings of the 25th Annual International Conference of the IEEE Engineering in Medicine and Biology Society (IEEE Cat. No.03CH37439), IEEE, Cancun, Mexico, 2003, pp. 3153–3156. URL: http://ieeexplore.ieee.org/document/1280811/. doi:10.1109/IEMBS.2003.1280811.

[39] A. Awad, M. Ghobashy, R. Stout, D. Silverman, K. Shelley, Blood pressure determination using the pulse oximeter waveform, 2001.

[40] Y. Li, Z. Wang, L. Zhang, X. Yang, J. Song, Characters available in photoplethysmogram for blood pressure estimation: beyond the pulse transit time, Australasian physical & engineering sciences in medicine 37 (2014) 367–376.

[41] K.-x. Zhang, Y. Wang, S. Zhang, Y.-m. Yang, Z.-c. Luo, Y.-j. Zeng, Dynamic analysis for blood flow parameters of cardiovascular system on work load, in: 2005 IEEE Engineering in Medicine and Biology 27th Annual Conference, IEEE, 2006, pp. 5551–5554.

[42] P. Salvi, C. Palombo, G. M. Salvi, C. Labat, G. Parati, A. Benetos, Left ventricular ejection time, not heart rate, is an independent correlate of aortic pulse wave velocity, Journal of Applied Physiology 115 (2013) 1610–1617. URL: http://www.physiology.org/doi/10.1152/japplphysiol.00475.2013. doi:10.1152/japplphysiol.00475.2013.

[43] C.-M. Huang, H.-C. Chang, S.-T. Kao, T.-C. Li, C.-C. Wei, C. Chen, Y.-T. Liao, F.-J. Chen, Radial Pressure Pulse and Heart Rate Variability in Heat- and Cold-Stressed Humans, Evidence-Based Complementary and Alternative Medicine 2011 (2011) 1–9. URL: http://www.hindawi.com/journals/ecam/2011/751317/. doi:10.1155/2011/751317.

[44] E. von Wowern, G. Östling, P. M. Nilsson, P. Olofsson, Digital photoplethysmography for assessment of arterial stiffness: repeatability and comparison with applanation tonometry, PloS one 10 (2015) e0135659.

[45] I. Imanaga, H. Hara, S. Koyanagi, K. Tanaka, Correlation between wave components of the second derivative of plethysmogram and arterial distensibility, Japanese heart journal 39 (1998) 775–784.

[46] T. Otsuka, T. Kawada, M. Katsumata, C. Ibuki, Utility of second derivative of the finger photoplethysmogram for the estimation of the risk of coronary heart disease in the general population, Circulation Journal 70 (2006) 304–310.

[47] H. J. Baek, J. S. Kim, Y. S. Kim, H. B. Lee, K. S. Park, Second derivative of photoplethysmography for estimating vascular aging, in: 2007 6th International Special Topic Conference on Information Technology Applications in Biomedicine, IEEE, 2007, pp. 70–72.

[48] V. Kazemi, J. Sullivan, One millisecond face alignment with an ensemble of regression trees, in: Proceedings of the IEEE conference on computer vision and pattern recognition, 2014, pp. 1867–1874.

[49] F. Bousefsaf, C. Maaoui, A. Pruski, Automatic Selection of Webcam Photoplethysmographic Pixels Based on Lightness Criteria, Journal of Medical and Biological Engineering 37 (2017) 374–385. URL: http://link.springer.com/10.1007/s40846-017-0229-1. doi:10.1007/s40846-017-0229-1.

[50] G. Lempe, S. Zaunseder, T. Wirthgen, S. Zipser, H. Malberg, Roi selection for remote photoplethysmography, in: Bildverarbeitung für die Medizin 2013, Springer, 2013, pp. 99–103.

[51] C. Sagonas, E. Antonakos, G. Tzimiropoulos, S. Zafeiriou, M. Pantic, 300 faces in-the-wild challenge: Database and results, Image and vision computing 47 (2016) 3–18.

[52] D. Djeldjli, F. Bousefsaf, C. Maaoui, F. Bereksi-Reguig, Imaging photoplethysmography: Signal waveform analysis, in: 2019 10th IEEE International Conference on Intelligent Data Acquisition and Advanced Computing Systems: Technology and Applications (IDAACS), volume 2, IEEE, 2019, pp. 830–834.

[53] M. Tarvainen, P. Ranta-aho, P. Karjalainen, An advanced detrending method with application to HRV analysis, IEEE Transactions on Biomedical Engineering 49 (2002) 172–175. URL: http://ieeexplore.ieee.org/document/979357/. doi:10.1109/10.979357.

[54] C. Rabbath, D. Corriveau, A comparison of piecewise cubic Hermite interpolating polynomials, cubic splines and piecewise linear functions for the approximation of projectile aerodynamics, Defence Technology 15 (2019) 741–757. URL: https://linkinghub.elsevier.com/retrieve/pii/S2214914719301187. doi:10.1016/j.dt.2019.07.016.

[55] G. Joseph, A. Joseph, G. Titus, R. M. Thomas, D. Jose, Photoplethysmogram (ppg) signal analysis and wavelet de-noising, in: 2014 annual international conference on emerging research areas: Magnetics, machines and drives (AICERA/iCMMD), IEEE, 2014, pp. 1–5.

[56] D. Castaneda, A. Esparza, M. Ghamari, C. Soltanpur, H. Nazeran, A review on wearable photoplethysmography sensors and their potential future applications in health care, International journal of biosensors & bioelectronics 4 (2018) 195.

[57] V. Hartmann, H. Liu, F. Chen, Q. Qiu, S. Hughes, D. Zheng, Quantitative comparison of photoplethysmographic waveform characteristics: effect of measurement site, Frontiers in physiology 10 (2019).

[58] A. V. Moco, S. Stuijk, G. De Haan, Ballistocardiographic artifacts in ppg imaging, IEEE Transactions on Biomedical Engineering 63 (2015) 1804–1811.

[59] M. V. Volkov, N. B. Margaryants, A. V. Potemkin, M. A. Volynsky, I. P. Gurov, O. V. Mamontov, A. A. Kamshilin, Video capillaroscopy clarifies mechanism of the photoplethysmographic waveform appearance, Scientific reports 7 (2017) 1–8.

[60] A. V. Moço, S. Stuijk, G. de Haan, New insights into the origin of remote ppg signals in visible light and infrared, Scientific reports 8 (2018) 1–15.